

## Comparative Study of Crystallite Size from XRD and TEM Results for Pure and V<sub>2</sub>O<sub>5</sub> Doped CdO-FePO<sub>4</sub> Composite Nanopowders

SK. Khaja Muswareen<sup>a,b</sup>, K. Venkatarao<sup>a,c</sup> and S. Cole<sup>a,\*</sup>

<sup>a</sup>Department of Physics, Acharya Nagarjuna University, Nagarjuna Nagar, Guntur-522510, A.P., India

<sup>b</sup>Department of Physics, P. B. Siddhartha College of Arts and Science, Vijayawada-520010, A.P., India

<sup>c</sup>Department of Physics, Government Institute of Textile Technology, Guntur-522005, A.P., India

(Received 12 April 2022, Accepted 6 June 2022)

CdO-FePO<sub>4</sub> composite nanopowders (CNPs) with V<sub>2</sub>O<sub>5</sub> ions as dopants are prepared by a sol-gel technique. The as-synthesized CNPs are characterized by peak profile analysis of powder X-ray diffraction (XRD) and Transmission electron microscopy (TEM). The powder XRD analysis reveals that the prepared products are crystalline with the cubic phase of CdO. The Debye-Scherrer's method and Williamson-Hall (W-H) plot analysis are worn to find out the separate contributions of the size of the crystal lattice and microstrain on the peak broadening of prepared CNPs. The other relevant physical parameters like microstrain and dislocation density values are determined for all the XRD peaks related to the cubic phase of CdO between 10 and 80 degrees of 2-theta values. The morphological analysis and determination of mean crystallite size are done from TEM images. The estimated crystallite size values obtained from the XRD (W-H plot and Debye-Scherrer's method) and TEM analysis revealed that the results are highly inter-correlated. The EDX spectra confirm the presence of elements Cd, Fe, P, V, and O in the prepared sample. FT-IR study exhibited functional groups related to phosphates and oxides.

**Keywords:** CdO-FePO<sub>4</sub> CNPs, V<sub>2</sub>O<sub>5</sub>, XRD, TEM, W-H method

### INTRODUCTION

Among the rapidly emerging developments in nanoscience & technology during the recent years, phosphate-based nanomaterials are acting as the best host materials owing to their good thermal, chemical, mechanical stability, self-activation, and low phonon energy [1]. Amongst the diverse phosphates, FePO<sub>4</sub> has very poor or low electrical conductivity due to its wide bandgap of about 4 eV [2]. The strong covalent bond between the P<sup>5+</sup> ions and oxygen to form the (PO<sub>4</sub>)<sup>3-</sup> group allows for good stabilization [3], greatly inhibiting high-rate applications in the fields of wastewater purification, high proton conductivity, corrosion protection, catalysis, as a positive electrode, etc. [4-6]. Accordingly, CdO is an n-type oxide

semiconductor having a direct bandgap energy value of 2.5 eV. The combination of varying amounts of two or more elements forms a binary/ternary single-phase inter-metallic solid with tuned parameters and can be used in diverse technological applications such as digital, magnetic drug delivery carriers, sensors, and storage devices [7]. Further, it is also been recognized that transition metal-doped FePO<sub>4</sub> might be worn as a good precursor for the preparation of LiFePO<sub>4</sub> for excellent electrochemical performances [8]. Some studies reported that the transition metals viz., Mg, Mn, Zn, and Al doping of FePO<sub>4</sub> [9] enhanced its properties. Besides, there were many research efforts to design hybrid nanostructures of FePO<sub>4</sub> by coating conductive materials like metals, metal oxides, and polymers via different synthetic routes or by substitution of supporting matrices to improve the FePO<sub>4</sub> conductivity [10].

On the other hand, the substitution of ferrites in

\*Corresponding author. E-mail: sandhya.cole@gmail.com

cadmium forms n-type semiconductors, and the raise of cadmium content results in a gradual decrease of the Seebeck coefficient. Also, Cd-Fe-based complex oxides are highly sensitive to ethanol gas over hydrogen, carbon monoxide, and isobutene [11]. T. Aswani *et al.* [12] synthesized Fe<sup>3+</sup> doped CdO nanopowders and studied their spectral characterization. Hu Zhou *et al.* [5] synthesized Graphene oxide-FePO<sub>4</sub> nanocomposite and characterized its photocatalytic properties. N. Kerkouri *et al.* [13] studied FTIR, Raman, EPR, and optical absorption spectra of V<sub>2</sub>O<sub>5</sub> doped cadmium phosphate glasses. P. Nagaraju *et al.* [14] studied Vanadium doped FePO<sub>4</sub> catalysts for the methyl pyrazine ammoxidation. Ian D. Johnson *et al.* [15] synthesized Vanadium doped LiFePO<sub>4</sub>/C nanocomposite high-rate cathodes for Li-ion batteries. K.S. Lohar *et al.* [16] synthesized Vanadium substituted Nickel Cadmium Ferrite by sol-gel method and studied their structural and magnetic properties. Recently some work has been done on spectroscopic studies of Mn<sup>2+</sup> doped CdO-Zn<sub>3</sub>(PO<sub>4</sub>)<sub>2</sub> nanocomposite synthesized by chemical precipitation method [17]. Despite the considerable studies available on Cd-Fe-based nanocomposite systems, as such, there are no studies on CdO-FePO<sub>4</sub> CNP. Thus the present research is aimed to couple CdO and FePO<sub>4</sub> to attain a novel CdO-FePO<sub>4</sub> CNP for its possible use in diverse potential applications like photo-catalyst, cathode material in rechargeable batteries. Further, among the all group-B transition metals V<sub>2</sub>O<sub>5</sub> is chosen as a dopant since VO<sup>2+</sup> is a stable molecular state compared to all the vanadium oxide family and also plays crucial role in phosphate metabolism [18]. After wide literature evaluation sol-gel method is adopted for the synthesis of CdO-FePO<sub>4</sub> CNPs with V<sub>2</sub>O<sub>5</sub> ions as dopants because this method requires low temperature, low cost, and easy compositional control to produce narrow size distribution and excellent crystalline structure [19].

The crystallite size and lattice strain are the two core properties of powder XRD peak width analysis. A size measure of coherently diffracting domains is called the crystallite size whereas a measure of the distribution of lattice constants occurring as of crystal imperfections (*viz.*, lattice dislocations, stacking faults, contact or sinter stresses, coherency stresses, and grain boundary triple junction) is termed as lattice strain [20]. Both of these

parameters affect the Bragg peak in diverse ways such as increasing the peak intensity & width and shifting in peak position ( $2\theta$ ). To determine the crystallite sizes and lattice strain, powder XRD remained a dominant method among the various techniques. There are various methods for quantitative analysis of XRD and determination of crystallite size and lattice strain *viz.*, Scherrer's equation, Warren-Averbach analysis, Williamson-Hall method, pseudo-Voigt function, and Rietveld refinement [21]. But still, Scherrer's equation is widely utilized when compared to W-H plot analysis for crystallite size and microstrain determination. TEM is also employed to observe the morphology and to measure the particle size of synthesized CNPs. In general, the crystallite size of the particles differs slightly from the particle size owing to the formation of poly-crystalline aggregates [22]. The present work is focused to report a comparative evaluation of the crystallite size from powder XRD procedures and the mean particle size of the CdO-FePO<sub>4</sub> CNPs with V<sub>2</sub>O<sub>5</sub> ions as dopants obtained from direct TEM measurements.

## Materials and Methods

In order to synthesize CdO-FePO<sub>4</sub> CNP by sol-gel route, high purity chemicals of Cadmium oxide (CdO) from Sigma-Aldrich Corp., Iron/Ferric Phosphate (FePO<sub>4</sub>), Vanadium Pentoxide (V<sub>2</sub>O<sub>5</sub>) from Merck Chemicals are chosen as preliminary resources without further purification. At first requisite stoichiometric proportions of precursors are dissolved in equal volumes of the deionized water-ethanol mixture and the solution was magnetically stirred at 1200 r.p.m for about 8 h until a homogeneous yellowish-brown color solution is obtained. During this continuous stirring NaOH dissolved in de-ionized water (which serves as pH controller and precipitating agent) is added to the above solution to obtain a homogeneous solution. Then after in order to remove further impurities, the solution was cleansed a few times with deionized water and later the precipitates were collected by centrifuging the mixture at 10,000 r.p.m for 30 min. Finally, the precipitate was allowed for subsequent calcination at 200 °C for 2 h in an annealing chamber operating at ambient pressure. A similar procedure is carried out for the synthesis of CdO-FePO<sub>4</sub> CNPs with V<sub>2</sub>O<sub>5</sub> ions as dopants while the V<sub>2</sub>O<sub>5</sub> dopant ions in a chosen stoichiometry (0.3, 0.6, and 0.9 mol%) are

added to the primary undoped solution during the stirring process. The as-synthesized nanocomposite was further used to analyze different spectroscopic characterizations.

### Characterization Techniques

The phase evaluation, the crystal size, and other physical parameters of the prepared CNPs are determined using Philips: PW1830 X-ray diffractometer instrument with 1.5406 Å wavelength-Cu-K $\alpha$  radiations in the range of 10°-80° (2 $\theta$ ) at a scanning rate of 2°/min upon maintaining the respective current 30 mA and operating voltage 40 kV. The morphology and mean particle size of the prepared CNPs are investigated using TEM (Hitachi HT7700 microscope) operated at 100 kV. A universal method for TEM sample preparation worn here is that the sample grid is set by dispersing the sample into ethanol with the assistance of ultrasonication; the droplets of the suspensions are deposited onto a carbon-enhanced copper grid and dried under a lamp in air. FEI Quanta FEG 200-HR-SEM of magnification ranging from 12x to greater than 1,00,000x is used to acquire EDX. Perkin Elmer Spectrum1: FT-IR Spectrometer is used to record FT-IR spectra of prepared CNPs mixed with KBr in the scanning range 4000-450 cm<sup>-1</sup>.

## RESULTS AND DISCUSSION

### Powder XRD Analysis

The powder XRD technique is employed for the phase investigation and purity of the as-synthesized products. The powder XRD patterns of the prepared CNPs are entirely consistent with the cubic phase of CdO with their reflection peaks at 33.02°, 38.38°, 55.34°, 65.93°, and 69.38° corresponding to the respective lattice planes (111), (200), (220), (311), (222) as indexed in Fig. 1 and are in accordance with the JCPDS 05-0640. The line broadening and sharp peaks signify that prepared samples are crystalline and are in nano-regime. No reflections of crystalline FePO<sub>4</sub> phases and dopant V<sub>2</sub>O<sub>5</sub> phases can be detected since the scattering domains are so small that the large line width of the reflections makes it impractical to discern them from the background [23] or it could be thought due to lower atomic radius of V<sub>2</sub>O<sub>5</sub> ~0.88 Å [24] and FePO<sub>4</sub> ~0.64 Å [25] when compared with CdO ~0.95 Å [26], they might have reacted with CdO and formed a stable

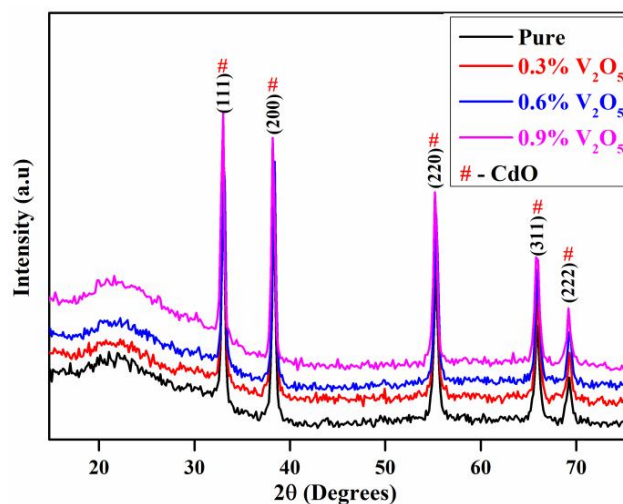


**Fig. 1.** XRD pattern of CdO-FePO<sub>4</sub> CNPs with V<sub>2</sub>O<sub>5</sub> as dopant ions.

solid with no secondary phases and with CdO as the predominant phase. A similar sort of XRD pattern is evidenced in Nanostructured Pt-FePO<sub>4</sub> thin-film electrodes wherein the presence of amorphous FePO<sub>4</sub> and nanocrystalline Pt in the Pt-FePO<sub>4</sub> thin films was confirmed by XRD [27]. It is also found that the XRD pattern is free from other peaks corresponding to impurity phases. Moreover, an adequate shift in the peak position and increase in intensity is evidenced in V<sub>2</sub>O<sub>5</sub> doped samples compared with pure samples indicating incorporation of VO<sup>2+</sup> ions into CdO-FePO<sub>4</sub> CNP, thereby influencing the microstructure and local disorder of prepared CNP. Figure 2 represents the slight shift and variation in intensity in predominant peak position 2 $\theta$  ~ 33.02° corresponding to the respective lattice plane (111) of the XRD pattern of pure and V<sub>2</sub>O<sub>5</sub> doped CdO-FePO<sub>4</sub> CNPs.

### Crystallite Size and Strain

Crystallite sizes and strain induced in the lattice of synthesized CNPs are estimated in comparison with Debye-Scherrer's and W-H plot method as follows

The crystallite size (D) is calculated from the well-known Debye-Scherrer's formula [28]

$$D = \frac{0.89\lambda}{\beta \cos \theta}$$

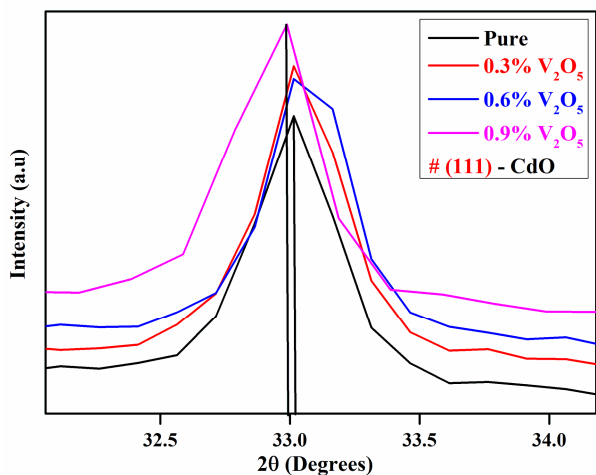


**Fig. 2.** Peak position shift and variation in the intensity of the predominant peak in the XRD pattern of CdO-FePO<sub>4</sub> CNPs with V<sub>2</sub>O<sub>5</sub> as dopant ions

Here  $\lambda$  is the wavelength of monochromatic Cu-K $\alpha$  radiation (1.5406 Å),  $\beta$  denotes Full Width at Half Maxima

(FW-HM) of the broad and intense peaks, and  $\theta$  is Bragg glancing angle related to (1 1 1) plane of XRD pattern.

The induced strain is deliberate using the Stokes-Wilson equation [29]

$$\varepsilon = \frac{\beta}{4 \tan \theta}$$

The graphical way of the W-H plot method [30] is used to calculate the mean crystallite size and microstrain of pure and V<sub>2</sub>O<sub>5</sub> doped CdO-FePO<sub>4</sub> CNPs by taking the width of a peak as a function  $2\theta$  from the expression as follows

$$\beta \cos \theta = (0.89\lambda/D) + 4\varepsilon \sin \theta$$

A graph is plotted between  $4 \sin \theta$  and  $\beta \cos \theta$  along x and y-axes respectively. The corresponding slope and intercept of the line give the value of microstrain and crystal size. Figure 3 depicts the W-H plot of pure and V<sub>2</sub>O<sub>5</sub> doped CdO-FePO<sub>4</sub> CNPs.

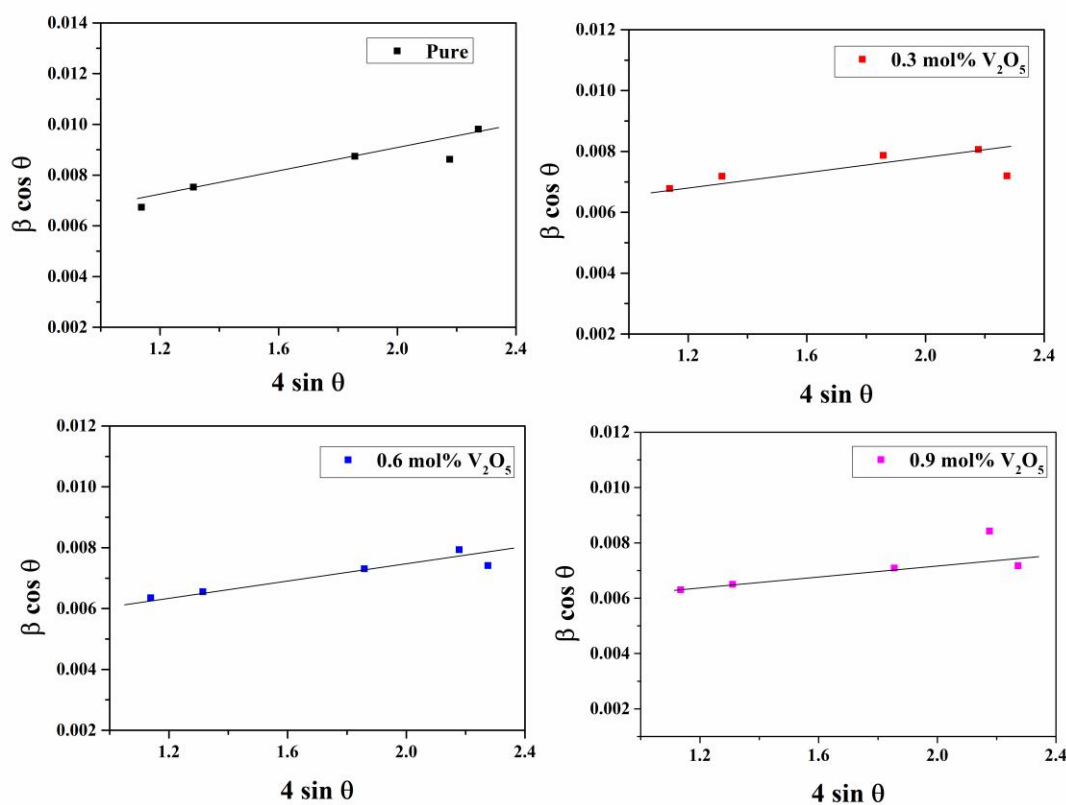


**Fig. 3.** Williamson-Hall plot of CdO-FePO<sub>4</sub> CNPs with V<sub>2</sub>O<sub>5</sub> as dopant ions.

The dislocation density values are evaluated using the equation  $\delta = 1/D^2$ . The determined values of crystallite sizes, induced microstrain, and relevant dislocation density parameters employing Debye-Scherrer's and W-H methods are tabulated in Table 1. From these obtained values, it has been practical that the crystallite size and lattice strain varied systematically with doping concentrations of  $V_2O_5$ , i.e., the crystallite size value increased slightly when compared with a pure sample upon increasing  $V_2O_5$  concentration. The dislocation density depends on the value of crystallite size. Furthermore, the cause of strain is consistent with lattice irregularity. Thus, the higher the value of microstrain, the lesser the crystallite size. This behaviour may be attributed to the shift in  $2\theta$  peak position & intensity, and increment/decrement in the Bragg peak width, caused by the tensile or compressive stress on the lattice derived from the incorporation of  $VO^{2+}$  ions into  $CdO-FePO_4$  CNP [31,32].

### TEM and EDX Analysis

The accuracy in the microstructure of the synthesized samples can be determined by a vital technique, TEM. TEM images of pure and  $V_2O_5$  doped  $CdO-FePO_4$  CNPs are illustrated in Fig. 4.

A keen view of the images demonstrates that the samples are exhibiting an assembly of spherical and rod structures of different diameters and sizes with little surface agglomerations. The agglomeration could be arisen due to the mutual interaction between the particles, electrostatic forces, and Vander walls forces [33]. The rod structures might be due to the  $CdO$  phase. Similar  $CdO$  nanorods have

been reported by Sumeet Kumar *et al.*, [34] synthesized by a co-precipitation method. The spherical structures could be due to the  $FePO_4$  phase. Similar  $FePO_4$  spherical structures have been reported by Jeannine Baumgartner *et al.*, [35]. It is reported that the particle shape usually contributes about 10% to the total lattice variation [36]. Here in this study, only a slight change in morphology of increase in rods is observed with an increase in doping concentration. Further, it is also reported that control of shape in transition metal nanostructures can be easily done with the help of stabilizing reagent which prevents the agglomeration of the nanostructures and uncontrolled growth [33].

The elemental chemical compositions of pure and  $V_2O_5$  doped  $CdO-FePO_4$  CNPs are analyzed by using EDX analysis and the corresponding recorded spectra are shown in Fig. 5. The EDX pattern confirms the existence of Cd, Fe, P, O in pure and Cd, Fe, P, O, V elements in  $V_2O_5$  doped  $CdO-FePO_4$  CNPs. It is apparent from the figure that no more peaks related to impurities or contaminants are noticed, which confirms the purity of the synthesized CNPs. The acquired compositions of elements Cd, Fe, P, O, and V that are certain in the table in the inset of Fig. 5 are in good concurrence with the experimental stoichiometric calculations. After the compositional analysis, it is noticed that the content of "V" is found to increase by varying  $V_2O_5$  doping concentration (0.3, 0.6, 0.9 mol%), signifying the replacement of Vanadium ions with other ions of the host lattice, without much disturbing the host lattice structure.

The mean particle sizes of the prepared CNPs are determined from TEM images by counting 50 particles in each sample to minimize errors and plotting histogram plots

**Table 1.** Average Crystallite Size, Lattice Strain, and Dislocation Density of  $CdO-FePO_4$  CNPs with  $V_2O_5$  as Dopant Ions from Debye-Scherrer's and W-H Plot Calculations

| Sample code | Crystallite size (nm) |          | Lattice strain ( $\epsilon \times 10^{-4}$ ) |          | Dislocation density ( $\delta$ ) $\times 10^{15}$ lines/m <sup>2</sup> |          |
|-------------|-----------------------|----------|--|----------|--|----------|
|             | Scherrer's            | W-H plot | Scherrer's                                   | W-H plot | Scherrer's   | W-H plot |
| $V_0$       | 20.39                 | 21.01    | 59.13  | 66.05    | 2.40   | 2.26     |
| $V_1$       | 20.46                 | 21.11    | 59.17  | 65.71    | 2.38   | 2.24     |
| $V_2$       | 21.92                 | 22.78    | 55.58  | 60.90    | 2.08   | 1.92     |
| $V_3$       | 22.01                 | 22.96    | 55.50  | 60.42    | 2.06   | 1.89     |

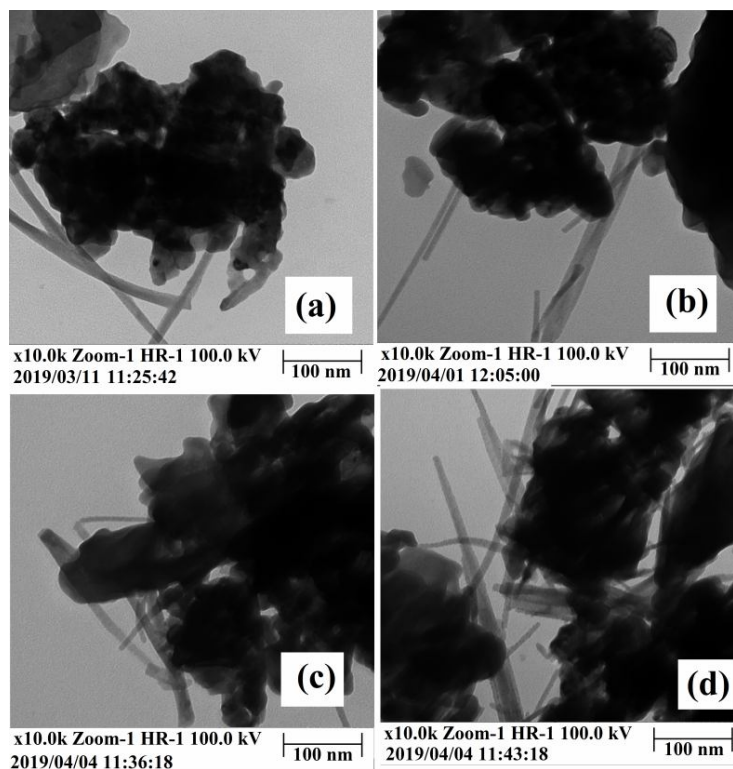


**Fig. 4.** TEM images of CdO-FePO<sub>4</sub> CNPs with V<sub>2</sub>O<sub>5</sub> as dopant ions (a) pure; (b) 0.3 mol% V<sub>2</sub>O<sub>5</sub>; (c) 0.6 mol% V<sub>2</sub>O<sub>5</sub>; (d) 0.9 mol% V<sub>2</sub>O<sub>5</sub> doped CdO-FePO<sub>4</sub> CNPs.

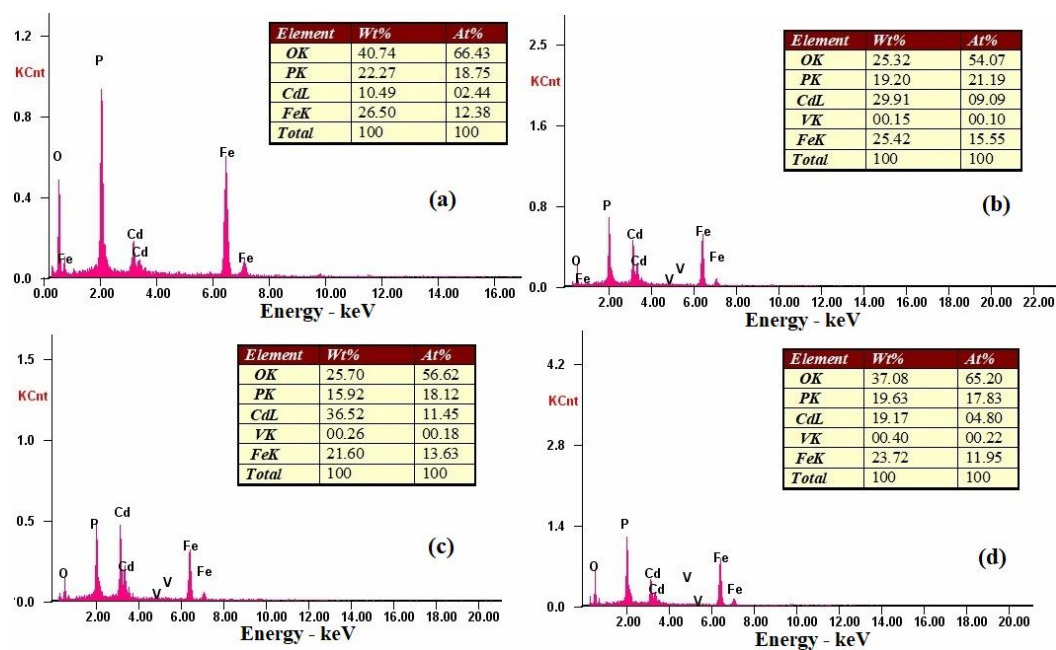


**Fig. 5.** EDX pattern of CdO-FePO<sub>4</sub> CNPs with V<sub>2</sub>O<sub>5</sub> as dopant ions (a) pure; (b) 0.3 mol% V<sub>2</sub>O<sub>5</sub>; (c) 0.6 mol% V<sub>2</sub>O<sub>5</sub>; (d) 0.9 mol% V<sub>2</sub>O<sub>5</sub> doped CdO-FePO<sub>4</sub> CNPs.



(Fig. 6) representing the estimated particle size distributions related to the measured diameters and measured widths of respective spheres and rods for all CdO-FePO<sub>4</sub> CNPs. The log normal distribution fit represented as a solid line in these figures corresponds to the value of the mean particle size of all CdOFePO<sub>4</sub> CNPs.

The as-obtained values of particle size of CdOFePO<sub>4</sub> CNPs from TEM images are deliberate in Table 2. From the complete TEM analysis, it is been practical that the morphology gets modified with more rods-like structures, and also the trend of increase in particle size as evidenced from XRD for higher concentrations of V<sub>2</sub>O<sub>5</sub> is followed in TEM analysis.

The crystallite sizes of CdOFePO<sub>4</sub> CNPs with V<sub>2</sub>O<sub>5</sub> as dopant ions as obtained from XRD analysis methods and TEM are given in Table 3. From the obtained results, it was noticed that the calculated size of crystallite by employing

**Table 2.** Average Particle Size Obtained from TEM Images of CdO-FePO<sub>4</sub> CNPs with V<sub>2</sub>O<sub>5</sub> as Dopant Ion

| Sample code    | Average particle size (nm) |
|----------------|----------------------------|
| V <sub>0</sub> | 23.49                      |
| V <sub>1</sub> | 21.86                      |
| V <sub>2</sub> | 25.79                      |
| V <sub>3</sub> | 28.12                      |

all these techniques is increased with increasing doping concentration. The crystallite size calculated by employing Debye-Scherrer's formula and W-H plot method is well fitted for the prepared CNPs when compared to the crystallite size estimated from TEM studies.

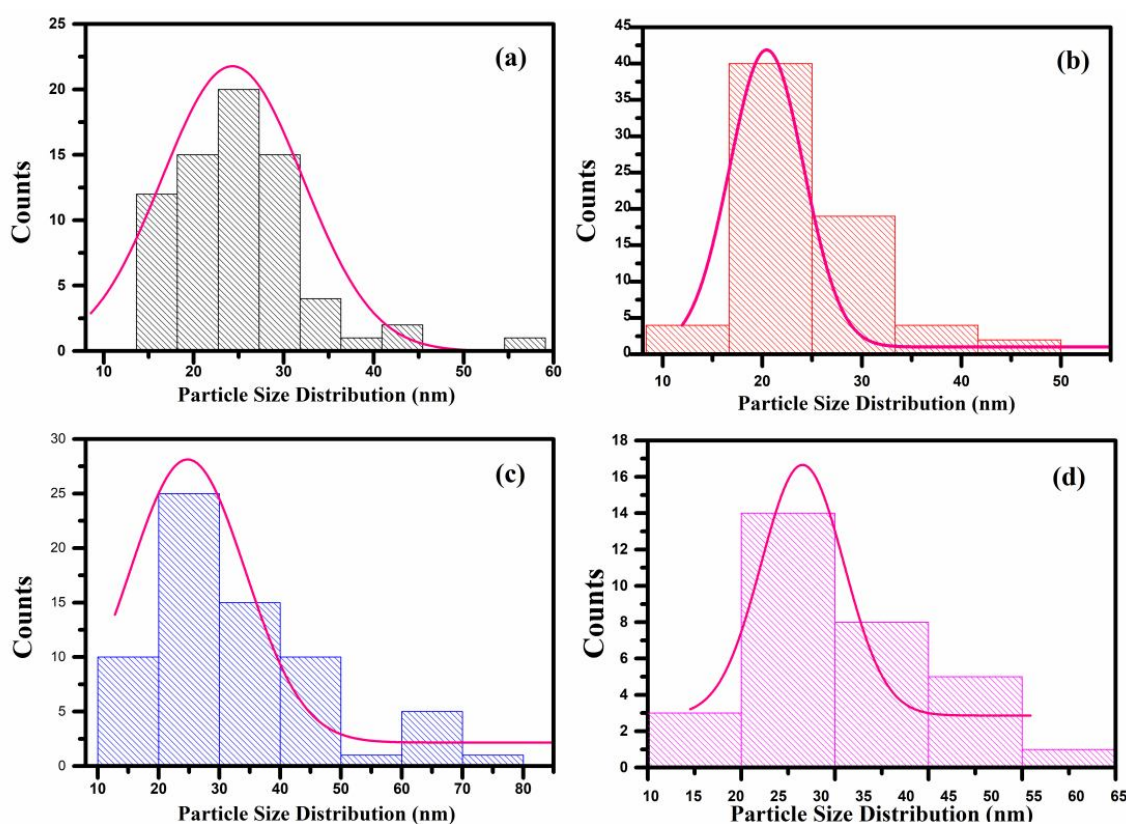


**Fig. 6.** Particle size distribution (nm) in CdO-FePO<sub>4</sub> CNPs with V<sub>2</sub>O<sub>5</sub> as dopant ions (a) pure; (b) 0.3 mol% V<sub>2</sub>O<sub>5</sub>; (c) 0.6 mol% V<sub>2</sub>O<sub>5</sub>; (d) 0.9 mol% V<sub>2</sub>O<sub>5</sub> doped CdO-FePO<sub>4</sub> CNPs.

**Table 3.** The Calculated Values of Crystallite Sizes Using XRD Methods and TEM Analysis

| Sample code    | Crystallite size (nm) |          | Particle size from TEM analysis (nm) |
|----------------|-----------------------|----------|--------------------------------------|
|                | Scherrer's method     | W-H plot |                                      |
| V <sub>0</sub> | 20.39                 | 21.01    | 23.49                                |
| V <sub>1</sub> | 20.46                 | 21.11    | 21.86                                |
| V <sub>2</sub> | 21.92                 | 22.78    | 25.79                                |
| V <sub>3</sub> | 22.01                 | 22.96    | 28.12                                |

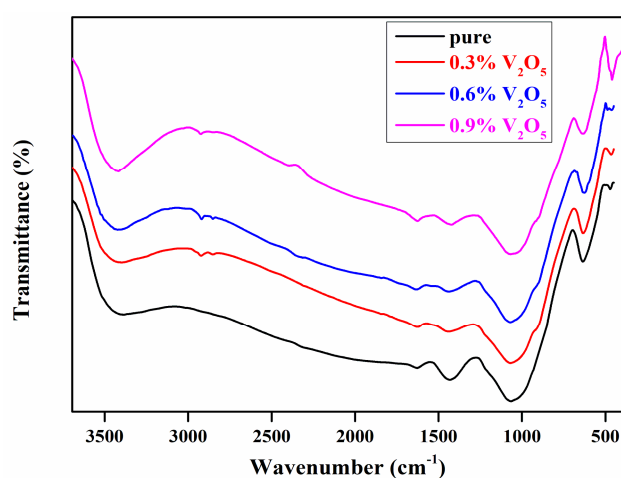
**Table 4.** FT-IR Vibrational Band Assignments of Pure and V<sub>2</sub>O<sub>5</sub> Doped CdOFePO<sub>4</sub> CNPs

| Pure | Wavenumber (cm <sup>-1</sup> )     |                                    |                                    | Assignment   |
|------|------------------------------------|------------------------------------|------------------------------------|--|
|      | 0.3% V <sub>2</sub> O <sub>5</sub> | 0.6% V <sub>2</sub> O <sub>5</sub> | 0.9% V <sub>2</sub> O <sub>5</sub> |  |
| 3427 | 3428                               | 3426                               | 3416                               | -OH stretching   |
| -    | 2922                               | 2922                               | 2920                               | -CH stretching   |
| 1631 | 1629                               | 1624                               | 1624                               | -OH bending  |
| 1431 | 1437                               | 1437                               | 1423                               | -CH <sub>2</sub> bending                                   |
| 1062 | 1062                               | 1069                               | 1057                               | Anti-symmetric stretching of PO <sub>4</sub> <sup>3-</sup> |
| -    | 885                                | 887                                | 886                                | Stretching mode of V-O-V                                   |
| 634  | 633                                | 631                                | 637                                | Symmetric P-O stretching                                   |
| 470  | 467                                | 464                                | 460                                | Metallic bonding of CdO                                    |

### FT-IR Analysis

The functional groups and chemical bonding in pure and V<sub>2</sub>O<sub>5</sub> doped CdO-FePO<sub>4</sub> CNPs are determined from FT-IR spectra shown in Fig. 7. The FT-IR spectrum exhibits a broad band at 3427 cm<sup>-1</sup> and a small band at 1630 cm<sup>-1</sup> due to stretching and bending vibrations of the O-H group linked chemically with CdO [37,38]. The OH/H<sub>2</sub>O functional group present in the system may be due to atmospheric water vapors. The transmittance peak at 2920 cm<sup>-1</sup> can be linked to C-H anti-symmetric vibration [39]. The bands observed at 1062 cm<sup>-1</sup> and 634 cm<sup>-1</sup> can be attributed to asymmetric stretching of PO<sub>4</sub><sup>3-</sup> ions and symmetric stretching of the P-O-P bridge [38,40]. The small bump observed at 885 cm<sup>-1</sup> in IR spectra of V<sub>2</sub>O<sub>5</sub> doped CdOFePO<sub>4</sub> CNPs corresponds to the stretching mode of V-O-V [41]. A peak at 470cm<sup>-1</sup> refers to the formation of Cd-O bonds [39]. The slight shift of most of the bands towards smaller wavenumber due to the incorporation of dopant is evidence of the physical interactions between CdO/FePO<sub>4</sub>/V<sub>2</sub>O<sub>5</sub> nanostructures. Table 4 gives a short-list

for tentative assignments of recognized band positions in FT-IR spectra of pure and V<sub>2</sub>O<sub>5</sub> doped CdOFePO<sub>4</sub> CNPs.

**Fig. 7.** FT-IR spectra of CdO-FePO<sub>4</sub> CNPs with V<sub>2</sub>O<sub>5</sub> as dopant ions.



## CONCLUSIONS

CdO-FePO<sub>4</sub> CNPs with V<sub>2</sub>O<sub>5</sub> as dopant ions are synthesized by a novel sol-gel route and are characterized by powder XRD and TEM. Powder XRD revealed that prepared samples belong to the cubic phase of CdO with crystalline nature in nano-dimension. The line broadening in diffraction peaks of CdOFePO<sub>4</sub> CNPs caused due to the lattice strain and small crystallite size are analyzed using Scherrer's formula, a graphical way of W-H analysis. The TEM image of prepared CNPs exhibited spherical and rod-like agglomerated structures with average particle sizes that are in good agreement with the results of Scherrer's and W-H methods. Apart from TEM imaging, XRD analysis still holds a dominant position in particle-size determination. FT-IR analysis confirms the presence of fundamental modes of host lattice and dopant ions.

## ACKNOWLEDGMENTS

The authors value the financial support from the Acharya Nagarjuna University for granting the University Research Fellowship that helped to carry out this research work.

## REFERENCES

- [1] Munirathnam, K.; Dillip, G. R.; Ramesh, B.; Joo, S. W.; Prasad Raju, B. D., Synthesis, photoluminescence and thermoluminescence properties of LiNa<sub>3</sub>P<sub>2</sub>O<sub>7</sub>:Tb<sup>3+</sup> green emitting phosphor. *J. Phys. Chem. Solids* **2015**, *86*, 170-176, <https://doi.org/10.1016/j.jpcs.2015.07.011>.
- [2] Zhou, F.; Kang, K.; Maxisch, T.; Ceder, G.; Morgan, D., The electronic structure and band gap of LiFePO<sub>4</sub> and LiMnPO<sub>4</sub>. *Solid State Commun.* **2004**, *132*, 181-186, <https://doi.org/10.1016/j.ssc.2004.07.055>.
- [3] Yoon, S.; Liao, C.; Sun, X. -G.; Bridges, C. A.; Unocic, R. R.; Nanda, J.; Dai, S.; Paranthaman, M. P., Conductive surface modification of LiFePO<sub>4</sub> with nitrogen-doped carbon layers for lithium-ion batteries. *J. Mater. Chem.* **2012**, *22*, 4611-4614, <http://dx.doi.org/10.1039/C2JM15325D>.
- [4] Hsu, K. -F.; Tsay, S. -Y.; Hwang, B. -J., Synthesis and characterization of nano-sized LiFePO<sub>4</sub> cathode materials prepared by a citric acid-based sol-gel route. *J. Mater. Chem.* **2004**, *14*, 2690-2695, <http://dx.doi.org/10.1039/B406774F>.
- [5] Zhou, H.; Yue, X.; Lv, H.; Kong, L.; Ji, Z.; Shen, X., Graphene oxide-FePO<sub>4</sub> nanocomposite: Synthesis, characterization and photocatalytic properties as a Fenton-like catalyst. *Ceram. Int.* **2018**, *44*, 7240-7244, <https://doi.org/10.1016/j.ceramint.2018.01.176>.
- [6] Lee, B.; Kim, C.; Park, Y.; Kim, T. -G.; Park, B., Nanostructured platinum/Iron phosphate thin-film electrodes for methanol oxidation. *Electrochem. Solid-State Lett.* **2006**, *9*, E27-E30, <http://dx.doi.org/10.1149/1.2256688>.
- [7] Gupta, M.; Gupta, M.; Anu; Mudsainiyan, R. K.; Randhawa, B. S., Physico-chemical analysis of pure and Zn doped Cd ferrites (Cd<sub>1-x</sub>Zn<sub>x</sub>Fe<sub>2</sub>O<sub>4</sub>) nanofabricated by pechini sol-gel method. *J. Anal. Appl. Pyrolysis* **2015**, *116*, 75-85, <https://doi.org/10.1016/j.jaap.2015.10.003>.
- [8] Wu, Z. -J.; Jiang, B. -F.; Liu, W. -M.; Cao, F. -B.; Wu, X. -R.; Li, L. -S., Selective recovery of valuable components from converter steel slag for preparing multidoped FePO<sub>4</sub>. *Ind. Eng. Chem. Res.* **2011**, *50*, 13778-13788, <https://doi.org/10.1021/ie202255g>.
- [9] Wu, Z. -J.; Zhou, Y.; Su, S. -H.; Gao, Z. -F.; Wu, X. -R.; Li, L. -S., A novel conversion of converter sludge into amorphous multi-doped FePO<sub>4</sub> cathode material for lithium ion batteries. *Scr. Mater.* **2012**, *67*, 221-224, <https://doi.org/10.1016/j.scriptamat.2012.04.027>.
- [10] Khaja Muswareen, S. K.; Cole, S., Influence of ZnO doping on spectral properties of sol-gel derived CdO-FePO<sub>4</sub> nanocomposites. *J. Electron. Mater.* **2021**, *50*, 1686-1698, <https://doi.org/10.1007/s11664-020-08534-8>.
- [11] Tianshu, Z.; Hing, P.; Jiancheng, Z.; Lingbing, K., Ethanol-sensing characteristics of cadmium ferrite prepared by chemical coprecipitation. *Mater. Chem. Phys.* **1999**, *61*, 192-198, [https://doi.org/10.1016/S0254-0584\(99\)00133-9](https://doi.org/10.1016/S0254-0584(99)00133-9).
- [12] Aswani, T.; Babu, B.; Manjari, V. P.; Stella, R. J.; Rao, G. T.; Krishna Ch, R.; Ravikumar, R. V. S. S. N., Synthesis and spectral characterizations of trivalent ions (Cr<sup>3+</sup>, Fe<sup>3+</sup>) doped CdO nanopowders.

- Spectrochim Acta A Mol. Biomol. Spectrosc.* **2014**, *121*, 544-550, <https://doi.org/10.1016/j.saa.2013.11.018>.
- [13] Kerkouri, N.; Haddad, M.; Et-tabirou, M.; Chahine, A.; Laâ nab, L., FTIR, Raman, EPR and optical absorption spectral studies on V<sub>2</sub>O<sub>5</sub>-doped cadmium phosphate glasses. *Phys. B: Condens. Matter* **2011**, *406*, 3142-3148, <https://doi.org/10.1016/j.physb.2011.04.057>.
- [14] Nagaraju, P.; Lingaiah, N.; Balaraju, M.; Sai Prasad, P. S., Studies on vanadium-doped iron phosphate catalysts for the ammoxidation of methylpyrazine. *Appl. Catal. A: Gen.* **2008**, *339*, 99-107, <https://doi.org/10.1016/j.apcata.2007.09.032>.
- [15] Johnson, I. D.; Lübke, M.; Wu, O. Y.; Makwana, N. M.; Smales, G. J.; Islam, H. U.; Dedigama, R. Y.; Gruar, R. I.; Tighe, C. J.; Scanlon, D. O.; Corà, F.; Brett, D. J. L.; Shearing, P. R.; Darr, J. A., Pilot-scale continuous synthesis of a vanadium-doped LiFePO<sub>4</sub>/C nanocomposite high-rate cathodes for lithium-ion batteries. *J. Power Sources* **2016**, *302*, 410-418, <https://doi.org/10.1016/j.jpowsour.2015.10.068>.
- [16] Lohar, K. S.; Patange, S.; Kulkarni, D.; Shirsath, S.; Jadhav, S.; S, S.; Kamble, S. R.; Mane, D., Structural and magnetic properties vanadium substituted nano nickel cadmium ferrites synthesized by sol-gel method. **2010**, NCANDT (Special Issue), 95.
- [17] Naga Bhaskararao, Y.; Satyavathi, K.; Subba Rao, M.; Cole, S., Synthesis and characterization of Mn<sup>2+</sup> doped CdOZn<sub>3</sub>(PO<sub>4</sub>)<sub>2</sub> nanocomposites. *J. Mol. Struct.* **2017**, *1130*, 585-591, <https://doi.org/10.1016/j.molstruc.2016.11.031>.
- [18] Rajyalakshmi, T.; Basha, S. J.; Khidhirbrahmendra, V.; Thampy, U. S. U.; Ravikumar, R. V. S. S. N., Synthesis and investigations for white LED material: VO<sup>2+</sup> doped Calcium Cadmium phosphate hydrate nanophosphor. *J. Mol. Struct.* **2020**, *1205*, 127605, <https://doi.org/10.1016/j.molstruc.2019.127605>.
- [19] Mustapha, S.; Ndamitso, M. M.; Abdulkareem, A. S.; Tijani, J. O.; Shuaib, D. T.; Mohammed, A. K.; Sumaila, A., Comparative study of crystallite size using Williamson-Hall and Debye-Scherrer plots for ZnO nanoparticles. *Adv. Nat. Sci.: Nanosci. Nanotechnol.* **2019**, *10*, 045013, <http://dx.doi.org/10.1088/2043-6254/ab52f7>.
- [20] Khorsand Zak, A.; Abd. Majid, W. H.; Abrishami, M. E.; Yousefi, R., X-ray analysis of ZnO nanoparticles by Williamson-Hall and size-strain plot methods. *Solid State Sci.* **2011**, *13*, 251-256, <https://doi.org/10.1016/j.solidstatesciences.2010.11.024>.
- [21] Rajesh Kumar, B.; Hymavathi, B., X-ray peak profile analysis of solid-state sintered alumina doped zinc oxide ceramics by Williamson-Hall and size-strain plot methods. *J. Asian Ceram. Soc.* **2017**, *5*, 94-103, <https://doi.org/10.1016/j.jascer.2017.02.001>.
- [22] Irfan, H.; Racik K, M.; Anand, S., Microstructural evaluation of CoAl<sub>2</sub>O<sub>4</sub> nanoparticles by Williamson-Hall and size-strain plot methods. *J. Asian Ceram. Soc.* **2018**, *6*, 54-62, <https://doi.org/10.1080/21870764.2018.1439606>.
- [23] Gerbaldi, C.; Meligrana, G.; Bodoardo, S.; Tuel, A.; Penazzi, N., FePO<sub>4</sub> nanoparticles supported on mesoporous SBA-15: Interesting cathode materials for Li-ion cells. *J. Power Sources* **2007**, *174*, 501-507, <https://doi.org/10.1016/j.jpowsour.2007.06.176>.
- [24] Satyavathi, K.; Subba Rao, M.; Nagabhaskararao, Y.; Cole, S., Synthesis, characterization of undoped and doped Zn<sub>3</sub>(PO<sub>4</sub>)<sub>2</sub>ZnO nanopowders by sol-gel method. *J. Mater. Sci. Mater. Electron.* **2017**, *28*, 1-13, <https://doi.org/10.1007/s10854-017-7038-8>.
- [25] Sayyar, Z.; Akbar Babaluo, A.; Shahrouzi, J. R. Kinetic study of formic acid degradation by Fe<sup>3+</sup> doped TiO<sub>2</sub> self-cleaning nanostructure surfaces prepared by cold spray. *Appl. Surf. Sci.* **2015**, *335*, 1-10, <https://doi.org/10.1016/j.apsusc.2015.01.014>.
- [26] Dakhel, A. A., Study of high mobility carriers in Ni-doped CdO films. *Bull. Mater. Sci.* **2013**, *36*, 819-825, <https://doi.org/10.1007/s12034-013-0535-3>.
- [27] Lee, B.; Kim, C.; Park, Y.; Kim, T. G.; Park, B., Nanostructured platinum/iron phosphate thin-film electrodes for methanol oxidation. *Electrochem. Solid-State Lett.* **2006**, *9*, E27-E30, <http://dx.doi.org/10.1149/1.2256688>.
- [28] Tiwary, C. S.; Sarkar, R.; Kumbhakar, P.; Mitra, A. K., Synthesis and optical characterization of monodispersed Mn<sup>2+</sup> doped CdS nanoparticles. *Phys. Lett. A* **2008**, *372*, 5825-5830,

- <https://doi.org/10.1016/j.physleta.2008.07.036>.
- [29] Stokes, A. R.; Wilson, A. J. C., The diffraction of X rays by distorted crystal aggregates-I. *Proc. Phys. Soc.* **1944**, *56*, 174-181, <https://doi.org/10.1088/0959-5309/56/3/303>.
- [30] Zhao, W.; Tian, C.; Xie, Z.; Wang, C.; Fu, W.; Yang, H., Hydrothermal growth of symmetrical ZnO nanorod arrays on nanosheets for gas sensing applications. *Front. Mater. Sci.* **2017**, *11*, 271-275, <https://doi.org/10.1007/s11706-017-0393-9>.
- [31] Sreedevi, G.; Srinivas, K.; Subbarao, M.; Cole, S., Investigation on structural and optical properties of CuO doped CdS-Zn<sub>3</sub>(PO<sub>4</sub>)<sub>2</sub> nanocomposite for optoelectronic devices. *J. Mol. Struct.* **2020**, *1222*, 128903. <https://doi.org/10.1016/j.molstruc.2020.128903>.
- [32] Madhavi, J. Comparison of average crystallite size by X-ray peak broadening and Williamson-Hall and size-strain plots for VO<sup>2+</sup> doped ZnS/CdS composite nanopowder. *SN Appl. Sci.* **2019**, *1*, 1509, <https://doi.org/10.1007/s42452-019-1291-9>.
- [33] Venugopalan, A.; Dhilip, M.; Krishnaswamy, S.; Sivakumar, K. S., Effect of transition metal ion substitution on structural and magnetic properties of Eu<sub>2</sub>O<sub>3</sub> sesquioxide system. *J. Mater. Sci. Mater. Electron.* **2017**, *28*, 12197-12206, <https://doi.org/10.1007/s10854-017-7035-y>.
- [34] Kumar, S.; Ahmed, B.; Ojha, A. K.; Das, J.; Kumar, A., Facile synthesis of CdO nanorods and exploiting its properties towards supercapacitor electrode materials and low power UV irradiation driven photocatalysis against methylene blue dye. *Mater. Res. Bull.* **2017**, *90*, 224-231, <https://doi.org/10.1016/j.materresbull.2017.02.044>.
- [35] Baumgartner, J.; Winkler, H. C.; Zandberg, L.; Tuntipopipat, S.; Mankong, P.; Bester, C.; Hilty, F.; Zeevaert, J. R.; Gowachirapant, S.; Zimmermann, M. B., Iron from nanostructured ferric phosphate: absorption and biodistribution in mice and bioavailability in iron deficient anemic women. *Sci. Rep.* **2022**, *12*, 2792, <https://doi.org/10.1038/s41598-022-06701-x>.
- [36] Qi, W. H.; Wang, M. P., Size and shape dependent lattice parameters of metallic nanoparticles. *J. Nanoparticle Res.* **2005**, *7*, 51-57, <https://doi.org/10.1007/s11051-004-7771-9>.
- [37] Mahjoore, M.; Aryafar, A.; Honarmand, M., Cadmium oxide nanoparticles as a novel photo-catalyst for degradation of ciprofloxacin antibiotic in aqueous media. *J. Min. Environ.* **2022**, *13*, 155-164, <https://doi.org/10.22044/jme.2022.11376.2120>.
- [38] Rao, M. S.; Satyavathi, K.; Naga Bhaskararao, Y.; Cole, S., Structural and spectral investigations of undoped and Mn<sup>2+</sup> ion doped Zn<sub>3</sub>(PO<sub>4</sub>)<sub>2</sub>ZnO nanocrystalline phosphor materials. *J. Alloys Compd.* **2016**, *682*, 7-13, <https://doi.org/10.1016/j.jallcom.2016.04.201>.
- [39] Prakash, T.; Ranjith Kumar, E.; Sumithra, M. G.; Alkhamis, K.; Munshi, A. M.; Mersal, G. A. M.; Shaaban, F.; El-Metwaly, N. M., Investigations of structural, morphological, optical and antimicrobial behaviour of Bi doped CdO nanostructures. *J. Inorg. Organomet. Polym. Mater.* **2022**, *32*, 280-288, <https://doi.org/10.1007/s10904-021-02127-6>.
- [40] Nirmal Rajeev, Y.; Venkatarao, K.; Naveen Kumar, B. V.; Bhushan Kumar, L.; Cole, S., Structural and morphological studies on strontium tin phosphate SrSn(PO<sub>4</sub>)<sub>2</sub> nanopowder. *Phys. Chem. Res.* **2022**, *10*, 267-271, <http://dx.doi.org/10.22036/pcr.2021.300514.1953>.
- [41] Surya Bhaskaram, D.; Cheruku, R.; Govindaraj, G., Reduced graphene oxide wrapped V<sub>2</sub>O<sub>5</sub> nanoparticles: green synthesis and electrical properties. *J. Mater. Sci. Mater. Electron.* **2016**, *27*, 10855-10863, <https://doi.org/10.1007/s10854-016-5194-x>.